Analysis of Reflective Cracks in Airfield Pavements Using a 3-D Generalized Finite Element Method

J. Garzon, C.A. Duarte† and W. Buttlar

Department of Civil and Environmental Engr.,
University of Illinois at Urbana-Champaign,
Newmark Laboratory,
205 North Mathews Avenue,
Urbana, IL 61801, USA
{jgarzon2,caduarte,buttlar}@illinois.edu

†*Corresponding Author*

RÉSUMÉ.

ABSTRACT. *Prediction and simulation of load-related reflective cracking in air field pavements require three-dimensional models in order to accurately capture the effects of gear loads on crack initiation and propagation. In this paper, we demonstrate that the Generalized Finite Element Method (GFEM) enables the analysis of reflective cracking in a three-dimensional setting while requiring significantly less user intervention in model preparation than the standard FEM. As such, it provides support for the development of mechanistic-based design procedures for airfield overlays that are resistant to reflective cracking.*
Two gear loading positions of a Boeing 777 aircraft are considered in this study. The numerical simulations show that reflective cracks in airfield pavements are subjected to mixed mode behavior with all three modes present. They also demonstrate that under some loading conditions, the cracks exhibit significant channeling.

MOTS-CLÉS :

KEYWORDS: *Fracture; Reflective cracks; Finite element method; Generalized finite element method; Extended finite element method*

1. Introduction

Very often, asphalt overlays are used to restore smoothness, structure, and waterproofing benefits to existing airfield pavements. However, the controlling factor for overlay lifespan is often reflective cracking in the new overlay caused by stress concentrations in the vicinity of joints and cracks in the underlying pavement. Reflective cracking can lead to roughness, spalling, and moisture infiltration at joints and cracks, which can greatly reduce the life expectancy of the overlay. Advanced spalling can also significantly increase FOD potential.

Historically, reflective cracking is thought to be driven by both thermal (non-load associated) and mechanical gear loading (load associated) forces [BOZ 02, KIM 02]. Tools are now available to aid the designer in the selection of an appropriate asphalt binder and mixture to resist thermally induced cracking. This includes both thermal (top-down) cracking [AAS09b, AAS09a], and thermally induced reflective cracking, or bottom-up cracks, emanating from the vicinity of cracks and joints in the underlying pavement [DAV 10]. However, recent research has indicated that the successful prediction and ability to design against reflective cracking lies in the ability to understand and account for load-related reflective cracking mechanisms [BAE 08, DAV 07]. Load-related reflective cracking mechanisms are more difficult to predict through modeling and simulation, as it is necessary to study this phenomenon in three dimensions (3-D) in order to accurately capture the effects of gear loads on crack initiation and propagation. Previous research has also demonstrated the need to directly account for the presence and propagation of cracks, in order to avoid mesh dependent numerical results. In a 3-D setting, this means that all modes of cracking must be considered, i.e., Mode I (opening), Mode II (shearing), and Mode III (tearing). The need for true 3-D modeling of reflective cracking complicates the development of computational models using standard finite element methods. The Generalized or Extended Finite Element Method [BAB 94, BAB 97, ODE 98, DUA 00, MO$\tilde{9}$9, SUK 00, MO$\tilde{0}$2] adds flexibility to the FEM while retaining its attractive features. A brief review of the Generalized FEM (*GFEM*) is presented in Section 3.

In this paper, we demonstrate that the *GFEM* enables the analysis of reflective cracking in a 3-D setting while requiring significantly less user intervention in model preparation. As such, it provides support for the development of mechanistic based design procedures for airfield overlays that are resistant to reflective cracking.

2. Formulation of Problem

In this paper, we analyze three dimensional reflective cracks assuming linear elastic isotropic material behavior. This section presents the strong and week formulations for this class of problem. The solution methodology based on the Generalized FEM (cf. Section 3) is, however, applicable to other material models, such as visco-elastic or visco-plastic behavior.

2.1. *Equilibrium Equations*

Consider a three-dimensional domain Ω with boundary $\partial\Omega$ decomposed as $\partial\Omega = \partial\Omega^u \cup \partial\Omega^\sigma$ with $\partial\Omega^u \cap \partial\Omega^\sigma = \emptyset$. The domain geometry is arbitrary and may have cracks. The equilibrium equations, constitutive and kinematic relations are given by

$$\begin{aligned} \bigtriangledown \cdot \boldsymbol{\sigma} + \boldsymbol{b} &= \mathbf{0} \quad \text{in } \Omega \\ \boldsymbol{\sigma} &= \boldsymbol{C} : \boldsymbol{\varepsilon} \\ \boldsymbol{\varepsilon} &= \bigtriangledown_s \boldsymbol{u} \end{aligned} \tag{1}$$

where $\boldsymbol{\sigma}$ is the Cauchy stress tensor, $\boldsymbol{b}$ are body forces, $\boldsymbol{\varepsilon}$ is the linear strain tensor, $\bigtriangledown_s$ is the symmetric part of the gradient operator and $\boldsymbol{C}$ is the Hooke's tensor. The material properties are assumed constant within each layer of the pavement (cf. Figure 7).

The boundary conditions prescribed in $\partial\Omega$ are as follows

$$\begin{aligned} \boldsymbol{u} &= \bar{\boldsymbol{u}} \quad \text{on } \partial\Omega^u \\ \boldsymbol{\sigma} \cdot \boldsymbol{n} &= \bar{\boldsymbol{t}} \quad \text{on } \partial\Omega^\sigma \end{aligned}$$

where $\boldsymbol{n}$ is an outward unit normal vector on $\partial\Omega$ and $\bar{\boldsymbol{u}}$ and $\bar{\boldsymbol{t}}$ are prescribed displacements and tractions, respectively.

2.2. *Weak Form*

The Principle of Virtual Work for the problem described above is given by

Find $\boldsymbol{u} \in H^1(\Omega)$ such that $\forall\, \boldsymbol{v} \in H^1(\Omega)$

$$\int_\Omega \boldsymbol{\sigma}(\boldsymbol{u}) : \boldsymbol{\varepsilon}(\boldsymbol{v}) d\boldsymbol{x} + \eta \int_{\partial\Omega^u} \boldsymbol{u} \cdot \boldsymbol{v} d\boldsymbol{s} = \int_{\partial\Omega^\sigma} \bar{\boldsymbol{t}} \cdot \boldsymbol{v} d\boldsymbol{s} + \eta \int_{\partial\Omega^u} \bar{\boldsymbol{u}} \cdot \boldsymbol{v} d\boldsymbol{s} \tag{2}$$

where $H^1(\Omega)$ is a Hilbert space defined on Ω and η is a penalty parameter. We use the penalty method to impose displacement boundary conditions due to its simplicity and generality. The computation of an approximation $\boldsymbol{u}^h$ of the solution $\boldsymbol{u}$ using the Generalized FEM is described in the next section.

3. The Generalized Finite Element Method

The Generalized FEM can be regarded as a finite element method with shape functions built using the concept of a partition of unity. This method has its origins in the works of Babuška et al. [BAB 94, BAB 97, MEL 96] (under the names "special finite element methods", "generalized finite element method" and "finite element partition of unity method") and Duarte and Oden [DUA 95, DUA 96b, DUA 96c, DUA 96a, ODE 98] (under the names "*hp* clouds" and "cloud-based *hp* finite element method").

Several meshfree methods proposed in recent years can also be viewed as special cases of the partition of unity method. Details on the mathematical formulation of the *GFEM* can be found in, e.g., [MEL 96, BAB 97, DUA 00, ODE 98, STR 01]. In this section, we summarize the main concepts of the method.

The linear finite element shape functions $\varphi_\alpha,\ \alpha = 1,\ldots,N$, in a finite element mesh with N nodes constitute a partition of unity, i.e.,

$$\sum_{\alpha=1}^{N} \varphi_\alpha(\boldsymbol{x}) = 1$$

for all $\boldsymbol{x}$ in a domain Ω covered by the finite element mesh. This is a key property used in partition of unity methods and, in particular, in the *GFEM*.

A *GFEM* shape function $\phi_{\alpha i}$ is built from the product of a FE shape function φ_α and an enrichment function $L_{\alpha i}$

$$\phi_{\alpha i}(\boldsymbol{x}) = \varphi_\alpha(\boldsymbol{x}) L_{\alpha i}(\boldsymbol{x}) \qquad (\text{no summation on } \alpha), \tag{3}$$

where α is a node in the finite element mesh. Figure 1 illustrates the construction of *GFEM* shape functions.

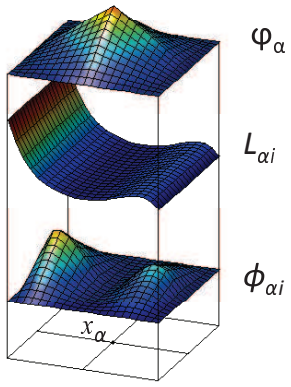

Figure 1. *Computation of a* GFEM *shape function (bottom surface). The finite element shape function φ_α is shown at the top, while the enrichment function $L_{\alpha i}$ is shown as the middle surface. The resulting function at the bottom, $\phi_{\alpha i}$ is the generalized FE shape function.*

This procedure allows the construction of shape functions which can approximate well the solution of a problem. Features such as discontinuities or material interfaces are represented by a judicious choice of enrichment functions $L_{\alpha i}(\boldsymbol{x})$, instead of finite element meshes with element faces fitting them.

Several enrichment functions can be hierarchically added to any node α in a finite element mesh. Thus, if D_L is the number of enrichment functions at node α, the GFEM approximation, $\boldsymbol{u}^h$, of a function $\boldsymbol{u}$ can be written as

$$\begin{aligned}\boldsymbol{u}^h(\boldsymbol{x}) &= \sum_{\alpha=1}^{N}\sum_{i=1}^{D_L}\underline{\boldsymbol{u}}_{\alpha i}\phi_{\alpha i}(\boldsymbol{x}) = \sum_{\alpha=1}^{N}\sum_{i=1}^{D_L}\underline{\boldsymbol{u}}_{\alpha i}\varphi_\alpha(\boldsymbol{x})L_{\alpha i}(\boldsymbol{x}) \\ &= \sum_{\alpha=1}^{N}\varphi_\alpha(\boldsymbol{x})\sum_{i=1}^{D_L}\underline{\boldsymbol{u}}_{\alpha i}L_{\alpha i}(\boldsymbol{x}) = \sum_{\alpha=1}^{N}\varphi_\alpha(\boldsymbol{x})\boldsymbol{u}^h_\alpha(\boldsymbol{x})\end{aligned}$$

where $\underline{\boldsymbol{u}}_{\alpha i},\ \alpha = 1,\ldots,N,\ i = 1,\ldots,D_L$, are nodal degrees of freedom and $\boldsymbol{u}^h_\alpha(\boldsymbol{x})$ is a local approximation of $\boldsymbol{u}$ defined on $\omega_\alpha = \{\boldsymbol{x}\in\Omega : \varphi_\alpha(\boldsymbol{x}) \neq 0\}$, the support of the partition of unity function φ_α. In the case of a finite element partition of unity, the support ω_α (often called a cloud or a patch) is given by the union of the finite elements sharing a vertex node $\boldsymbol{x}_\alpha$ [DUA 00]. The GFEM approximation $\boldsymbol{u}^h$ is the solution of the following problem

Find $\boldsymbol{u}^h \in \boldsymbol{X}^h(\Omega) \subset H^1(\Omega)$ such that, $\forall\ \boldsymbol{v}^h \in \boldsymbol{X}^h(\Omega)$

$$\int_\Omega \boldsymbol{\sigma}(\boldsymbol{u}^h) : \boldsymbol{\varepsilon}(\boldsymbol{v}^h)d\boldsymbol{x} + \eta\int_{\partial\Omega^u}\boldsymbol{u}^h\cdot\boldsymbol{v}^h d\boldsymbol{s} = \int_{\partial\Omega^\sigma}\bar{\boldsymbol{h}}\cdot\boldsymbol{v}^h d\boldsymbol{s} + \eta\int_{\partial\Omega^u}\bar{\boldsymbol{u}}\cdot\boldsymbol{v}^h d\boldsymbol{s} \qquad (4)$$

where, $\boldsymbol{X}^h(\Omega)$ is a subspace of $H^1(\Omega)$ generated by the GFEM shape functions defined in (3).

The local approximations $\boldsymbol{u}^h_\alpha,\ \alpha = 1,\ldots,N$, belong to local spaces $\chi_\alpha(\omega_\alpha) = \text{span}\{L_{i\alpha}\}_{i=1}^{D_L}$ defined on the supports $\omega_\alpha,\ \alpha = 1,\ldots,N$. The selection of the enrichment or basis functions for a particular local space $\chi_\alpha(\omega_\alpha)$ depends on the local behavior of the function $\boldsymbol{u}$ over the cloud ω_α. The case of 3-D fractures is discussed below.

3.1. *Enrichment functions for 3-D cracks*

In this section, enrichment functions for 3-D cracks are briefly described. Further details can be found in [PER 09a]. Three types of enrichment functions are considered :

(i) Enrichment for clouds ω_α that do not intersect the crack surface.

In this case, the elasticity solution $\boldsymbol{u}$ is continuous and can be approximated by polynomial functions. Our implementation follows [ODE 98, DUA 00] and the enrichments functions $\{L_{\alpha i}\}_{i=1}^{D_L}$ for a cloud associated with node $\boldsymbol{x}_\alpha = (x_\alpha, y_\alpha, z_\alpha)$ is given by

$$\{L_{\alpha i}\}_{i=1}^{D_L} = \left\{1, \frac{(x-x_\alpha)}{h_\alpha}, \frac{(y-y_\alpha)}{h_\alpha}, \frac{(z-z_\alpha)}{h_\alpha}, \frac{(x-x_\alpha)^2}{h_\alpha^2}, \frac{(y-y_\alpha)^2}{h_\alpha^2}, \ldots\right\} \qquad (5)$$

with h_α being a scaling factor [ODE 98, DUA 00].

(ii) Enrichment for clouds completely cut by the crack surface.

In this case, the crack surface divides ω_α into two sub-domains, ω_α^+ and ω_α^- such that $\omega_\alpha = \omega_\alpha^+ \cup \omega_\alpha^-$. The enrichments functions are taken as

$$\{L_{\alpha i}\}_{i=1}^{D_L} = \left\{ \mathscr{H}, \mathscr{H}\frac{(x-x_\alpha)}{h_\alpha}, \mathscr{H}\frac{(y-y_\alpha)}{h_\alpha}, \mathscr{H}\frac{(z-z_\alpha)}{h_\alpha}, \mathscr{H}\frac{(x-x_\alpha)^2}{h_\alpha^2}, \mathscr{H}\frac{(y-y_\alpha)^2}{h_\alpha^2}, \dots \right\} \tag{6}$$

where the function $\mathscr{H}(\boldsymbol{x})$ denotes a discontinuous function defined by

$$\mathscr{H}(\boldsymbol{x}) = \begin{cases} 1 & \text{if } \boldsymbol{x} \in \omega_\alpha^+ \\ 0 & \text{otherwise} \end{cases} \tag{7}$$

These discontinuous functions can approximate discontinuities of the elasticity solution $\boldsymbol{u}$ *inside* a finite element.

(iii) Enrichment for clouds that intersect the crack front.

Terms from the asymptotic expansion of the elasticity solution near crack fronts are used as enrichment functions in clouds that intersect the crack front. Their description is more elaborated than the previous ones and we refer the interested reader to references [PER 09a, DUA 00, DUA 01].

With the above enrichments, the finite element mesh is not required to fit crack surfaces since the discontinuities and singularities are approximated by the enrichment functions, not the FEM mesh. This is in contrast with the FEM and greatly facilitate the solution of fracture mechanics problems in complex 3-D domains such as those found in airfield pavements. This feature of the GFEM is illustrated in Figures 2 and 11.

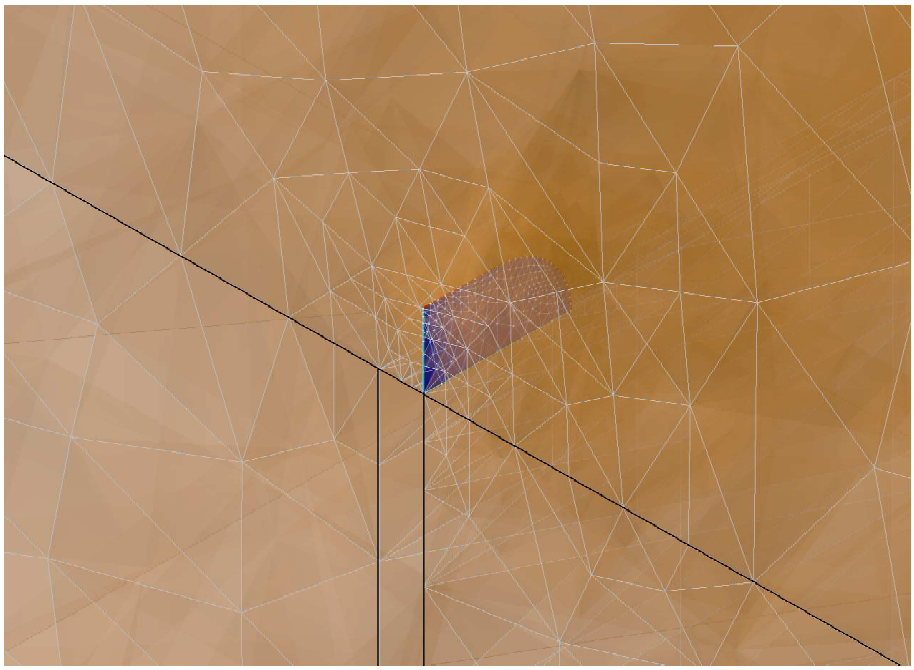

Figure 2. *Three-dimensional crack in a pavement. The crack can be inserted into an existing finite element mesh without requiring modifications on the FE mesh originally designed to represent an uncracked pavement. The crack is approximated by discontinuous enrichment functions, not the FEM mesh.*

4. Inclined elliptical crack

This example is aimed at verifying the *GFEM* methodology in a mixed mode fracture case. The problem consists of an inclined elliptical crack of dimensions $a/c = 9/15$ embedded in a cube of edge size b, as illustrated in Figure 3. In order to reduce the finite domain effect on the solution, the relation $c/b = 3/40$ is set. The Young's modulus used in this example is $E = 1.0$ while the Poisson's ratio is set to $\nu = 0.25$. The crack surface has an inclination $\alpha = 30^\circ$ with respect to the horizontal axis. The domain is subjected to a uniform tensile traction $\sigma_\circ = 1$ in the vertical direction. Figure 3 shows the model and the initial coarse mesh used in this example. In the discretization of the solution, localized mesh refinement on elements that intersect the crack front is applied along with nodal enrichments. Polynomial enrichment of order $p = 3$ (cf. Eq. (5)) is applied over the entire domain , discontinuous step function enrichment (cf. Eq. (6)) is applied at the nodes of the elements that are cut by the crack surface and the asymptotic solution enrichment is used at elements cut by the crack front. The ratio of the element size, L, to crack length, a, for elements along the crack front is $0.054 < L/a < 0.088$ after the mesh refinement is applied.

The stress intensity factors for modes I, II, and III of an inclined elliptical crack embedded in an infinite domain are used as references. These SIFs are given by [TAD 00]

$$
\begin{aligned}
K_I^{\text{inf.}} &= \frac{\sigma_\circ \sin^2\gamma\sqrt{\pi a}}{E(k)}\left[\sin^2\theta + \left(\frac{a}{c}\right)^2\cos^2\theta\right]^{\frac{1}{4}} \\
K_{II}^{\text{inf.}} &= -\frac{\sigma_\circ \sin\gamma\cos\gamma\sqrt{\pi a}k^2}{\left[\sin^2\theta + \left(\frac{a}{c}\right)^2\cos^2\theta\right]^{\frac{1}{4}}}\left[\frac{k'}{B}\cos\omega\cos\theta + \frac{1}{C}\sin\omega\sin\theta\right] \\
K_{III}^{\text{inf.}} &= \frac{\sigma_\circ \sin\gamma\cos\gamma\sqrt{\pi a}(1-\nu)k^2}{\left[\sin^2\theta + \left(\frac{a}{c}\right)^2\cos^2\theta\right]^{\frac{1}{4}}}\left[\frac{1}{B}\cos\omega\sin\theta - \frac{k'}{C}\sin\omega\cos\theta\right]
\end{aligned}
$$

where B, C, $K(k)$ and $E(k)$ are defined as

$$
\begin{aligned}
&B = (k^2-\nu)E(k) + \nu k' K(k), \quad C = (k^2-\nu k'^2)E(k) - \nu k'^2 K(k), \\
&K(k) = \int_0^{\frac{\pi}{2}} \frac{d\varphi}{\sqrt{1-k^2\sin^2\varphi}}, \qquad E(k) = \int_0^{\frac{\pi}{2}} \sqrt{1-k^2\sin^2\varphi}\, d\varphi\ ,
\end{aligned}
$$

and $k^2 = 1-k'^2$, $k' = a/c$ and θ is a parametric angle representing a point A on the crack front (cf. Figure 3). For the example solved in this section, $\gamma = \pi/2 - \alpha = \pi/3$ and $\omega = 0$.

The extracted stress intensity factors for mode I, II, and III using the *GFEM* methodology are presented in Figure 4. These results are compared with the analytical

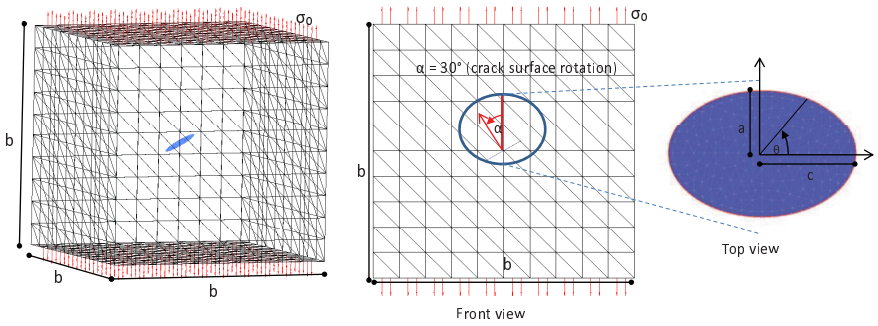

Figure 3. *Cube subjected to top and bottom uniform tensile tractions and representation of inclined elliptical crack.*

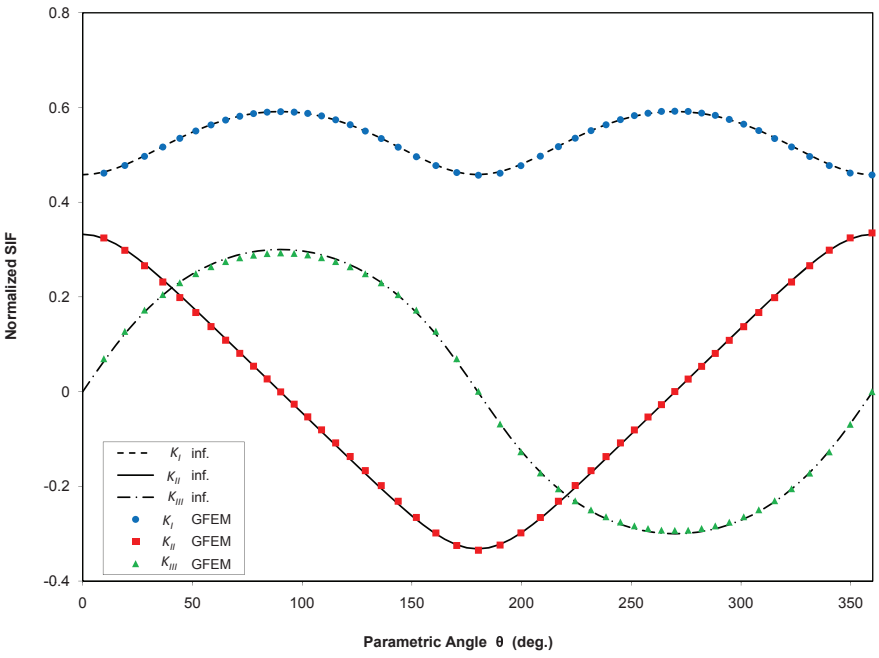

Figure 4. *Stress intensity factors for modes I, II, and III.*

solution for an infinite domain and excellent agreement can be observed between the two solutions for all three modes.

5. Analysis of Reflective Cracks in Airfield Pavements

Since the purpose of this study is to analyze rather than design a typical pavement section of an airport that serves the Boeing 777 aircraft was selected to be modeled. The model geometry and pavement cross sections for the underlying PCC are arbitrarily selected as the standard section of runway 4L-22R at O'Hare Airport.

A three-dimensional finite element mesh was created to represent the airport pavement and its layers. Also, a two-dimensional finite element mesh was created to represent the geometry of the crack surface. By modeling the 3-D pavement mesh and inserting the 2-D crack surface mesh just above the concrete joint, a reflective cracking study in asphalt overlay was performed with The Generalized Finite Element Method described in the previous section. Modes I, II and III stress intensity factors are computed along the crack front in order to investigate the three-dimensional, mixed mode crack driving mechanisms in a typical airfield pavement.

5.1. *Model Geometry*

The pavement model encompasses half of two adjacent slabs and one PCC joint as illustrated by the shaded region in Figure 5. The simulated airfield pavement is composed of an 20 cm asphalt overlay ; 23 cm concrete slabs, each with plan dimensions of 6 m $\times$ 5.7 m (PCC), and ; an 28 cm cement treated base (CTB). A saw cut of 13 mm width is modeled in the PCC layer.

The dimensions of the crack surface are 2.54 cm of hight and 5 cm of depth. The curved portion of the crack has a radius of 2.54 cm and starts and the midpoint of its depth. Figure 6 shows the geometry of the crack surface.

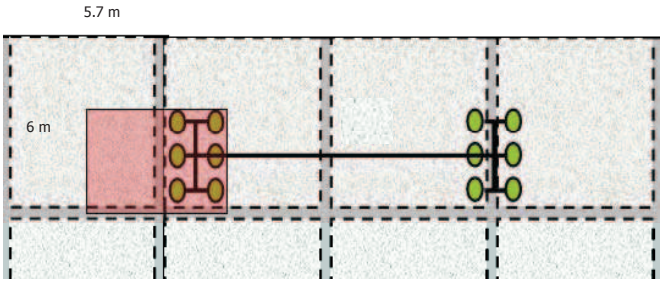

Figure 5. *Airfield pavement analyzed. The shaded square represents the portion of pavement modeled in this study.*

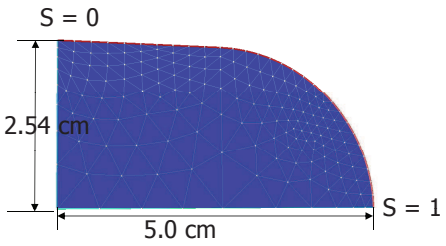

Figure 6. *Reflective crack geometry details.*

5.2. *Material Properties*

All layers are assumed to have elastic material properties for the purpose of simplifying preliminary modeling. The asphalt overlay modulus of elasticity was taken as 1,379 MPa, with a Poisson's ratio of 0.35. The concrete slabs were assumed to have a Young's modulus of 27,579 MPa, while the CTB modulus was taken as 6,895 MPa. The Poisson's ratio for the concrete slabs and the CTB layer were assumed to be 0.15 and 0.20, respectively. Figure 7 show details of the pavement considered.

Furthermore, the interface between asphalt overlay and Portland cement concrete layer was assumed to be fully bounded.

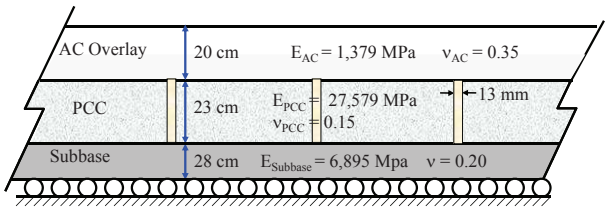

Figure 7. *Material properties and details of a standard section of runway 4L-22R at O'Hare Airport.*

5.3. *Loading Details*

The Boeing 777-200 aircraft has two main landing gears with a main gear width of 11 m. Due to the very large width of the gear, we assume here that the distance between gears is large enough such that interactions may be neglected for the purposes of studying the mixed mode behavior and 3-D responses. One side of the dual-tridem main gear carries about the 47.5% of the gross taxiway weight (288 Ton) of the Boeing 777-200 aircraft, and is composed of six wheels with an individual contact tire pressure of 1,482 MPa [ADM 95]. Details are shown in Figure 8.

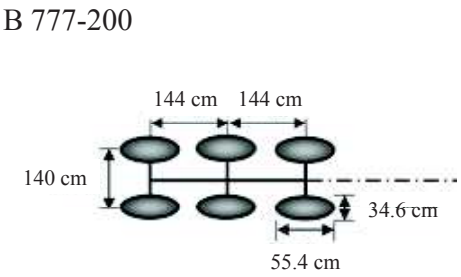

Figure 8. *Boeing 777-200 aircraft wheel loading detail.*

Two gear loading positions of the aircraft are considered in this study as shown in Figure 9. Load Position A (Cf. Figure 9(a)) loads the pavement symmetrically with respect to the PCC joint, while Position B leads to strong shear deformations at the PCC joint. These loading configurations are expected to show different fracture deformation modes and provide information about possible crack growth mechanisms.

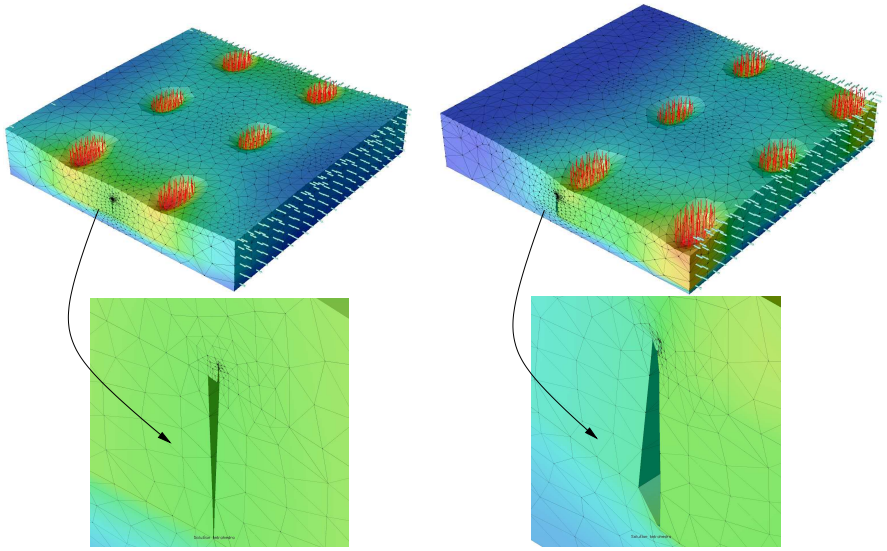

(a) Load position A and corresponding deformed configuration at the PCC joint.

(b) Load position B and corresponding deformed configuration at the PCC joint.

Figure 9. *Gear load positions considered in this study. Position A loads the pavement symmetrically with respect to the PCC joint while Position B leads to strong shear deformations at the PCC joint.*

5.4. *Finite Element Mesh Details*

A relatively coarse 3-D mesh *without any crack discretization* was created using the software program Patran [PAT]. Thus, finite element meshes with element faces fitting the crack surface are not needed. This greatly simplifies the construction of 3-D meshes, enabling, for example, parametric studies and simulations of crack growth. Furthermore, the generation of elements with good aspect ratios is also facilitated. Smaller elements were created around the PCC joint and locations where wheel loads are applied, as shown in Figures 10(a) and 10(b), respectively.

Two-dimensional triangular elements are used to represent the geometry of the crack surface as illustrated in Figure 6. These elements are also used to define discontinuous enrichment functions, which are able to represent the solution inside elements cut by the crack surface. Details on these functions are described in [PER 09a, PER 09b, DUA 01]. The 2-D elements do not have any degrees of freedom. Furthermore, the crack triangulation is completely independent of the 3-D mesh.

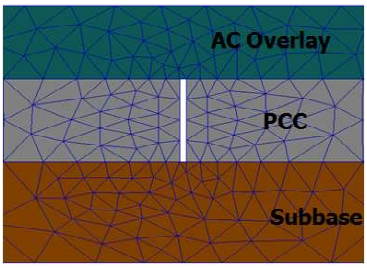

(a) Tetrahedral mesh around PCC joint.

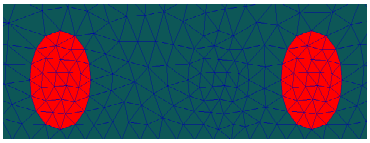

(b) Discretization around locations where wheel loads are applied.

Figure 10. *Details of discretization used in the* GFEM *model.*

5.5. GFEM *Procedure*

In order to perform a three-dimensional analysis of reflective cracking in a airfield pavements; the 3-D FEM model loaded with one main gear of a Boeing 777 aircraft is simulated using the Generalized Finite Element Method. A reflective crack is inserted at the bottom of the asphalt overlay for the purpose of the stress intensity factor and the energy release rate investigation. The finite element generated in Patran was loaded into a *GFEM* code developed at the University of Illinois. The mesh was then automatically refined around the crack front in order to obtain accurate stress intensity factors. The ratio of characteristic element size to crack radius, L_e/a, along the crack front was $0.004 \leq L_e/a \leq 0.1$. Even though this ratio may seem large compared to what is normally used in finite element models for 3-D cracks, the *GFEM* is able to deliver accurate solutions due to the analytical enrichments used at nodes near the

crack front. Third and fourth order polynomial shape functions were also used to approximate the continuous part of the solution [PER 09a, PER 09b]. Figure 11 shows the resulting tetrahedral mesh used in the model along with a detailed view in at the location where the crack was inserted. Extraction of stress intensity factors was performed using the Cut-off Function Method (CFM) [SZA 88, PER 05]. Extraction was performed for the opening mode (Mode I), shearing mode (Mode II) and tearing mode (mode III) stress intensity factors.

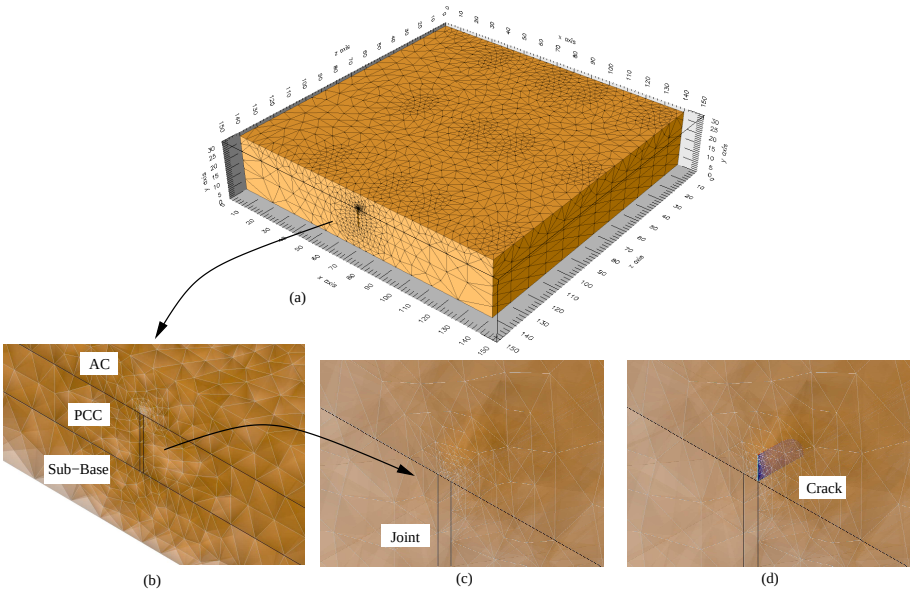

Figure 11. *Modeling of a 3-D reflective crack with the Generalized FEM. The crack is modeled using discontinuous and singular* GFEM *shape functions, instead of a finite element mesh with element faces oriented with the crack. (a) 3-D mesh without crack. (b) and (c) Details of mesh in vicinity of joint. (d) Reflective crack inserted into existing uncracked FE mesh.*

5.6. *Analysis of Results*

Figures 12 and 13 show the stress intensity factors (SIFs) and energy release rate (J), respectively, along the crack front for load position A. We can observe that this is clearly a mode I dominated case and that K_I and J vary significantly along the crack front reaching a maximum value at $s = 1$, where s is a non-dimensional coordinate along the crack front. This demonstrates that, under this loading, the crack will grow faster at $s = 1$ than at $s = 0$ and thus it will exhibit significant channeling behavior. The non-zero K_{II} and K_{III} shown in Figure 12 are caused by the fact that the crack was inserted above the right hand side of the PCC joint, as illustrated in Figure 9(a). Furthermore, the tetrahedral mesh is highly unstructured and thus the loads applied on element faces are not symmetrical with respect to the center line of the PCC joint (the plane of symmetry). The values of K_{II} and K_{III} are also considered for the computation of the energy release rate (J) even thought their contributions are very small compared to the contribution of mode I.

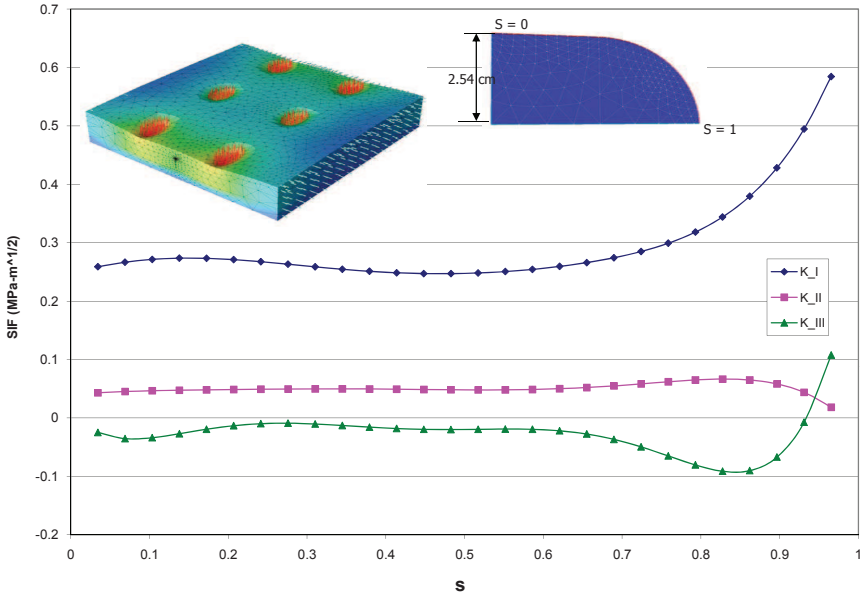

Figure 12. *Stress Intensity Factors (SIFs) along crack front for load position A.*

Figures 14 and 15 show the same results as above but for load position B. The distribution of SIFs along the crack front is significantly different from that of load position A. We can observe an interplay between Mode II and Mode III behavior. At $s = 0$ Mode II dominates while at $s = 1$ Mode III dominates and Mode II is close to zero. Figure 15 shows the energy release rate contributions from K_{II}, the shearing mode, and K_{III}, the tearing mode. We can observe that as the K_{II} contribution goes

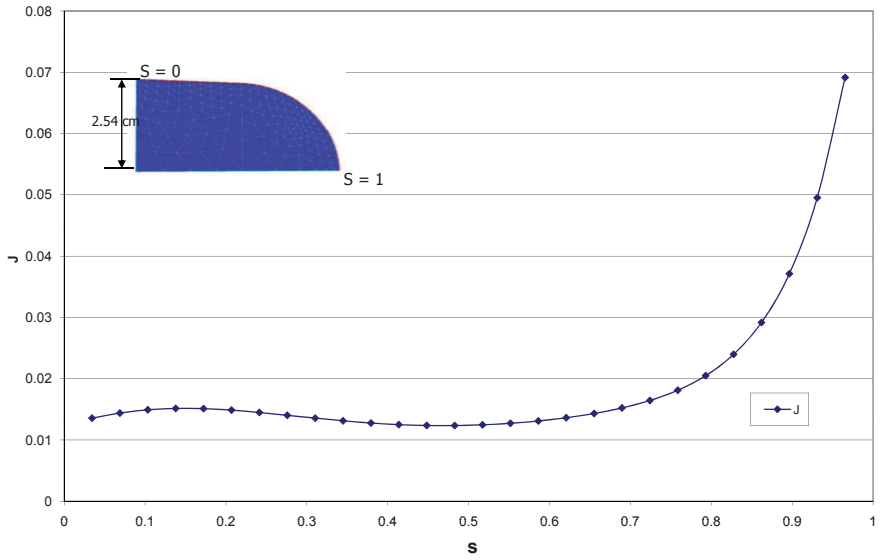

Figure 13. *Energy contributions from each mode for load position A.*

to zero as s increases, K_{III} contribution increases. Thus, at $s = 0$ the crack will grow by shear action while at $s = 1$ it will need to tear the material in order to grow. This decrease in values for K_{II} and increase for K_{III}, is due to the fact that the crack front changes direction. It starts as a horizontal line in the YZ plane but it curves and becomes almost a vertical line in the same plane. If the crack front were to stay in the horizontal direction K_{II} would remain being the dominate case in this example.

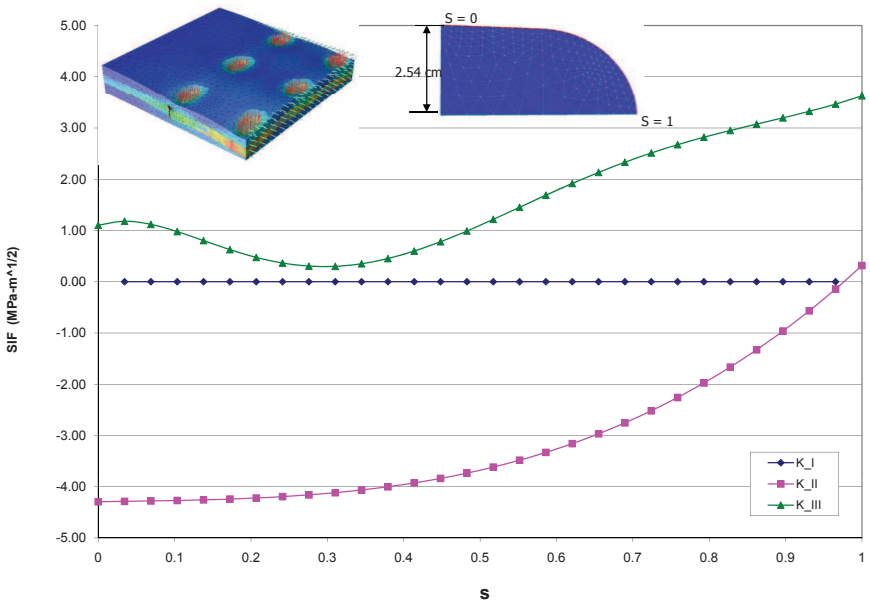

Figure 14. *Stress Intensity Factors (SIFs) along crack front for load position B.*

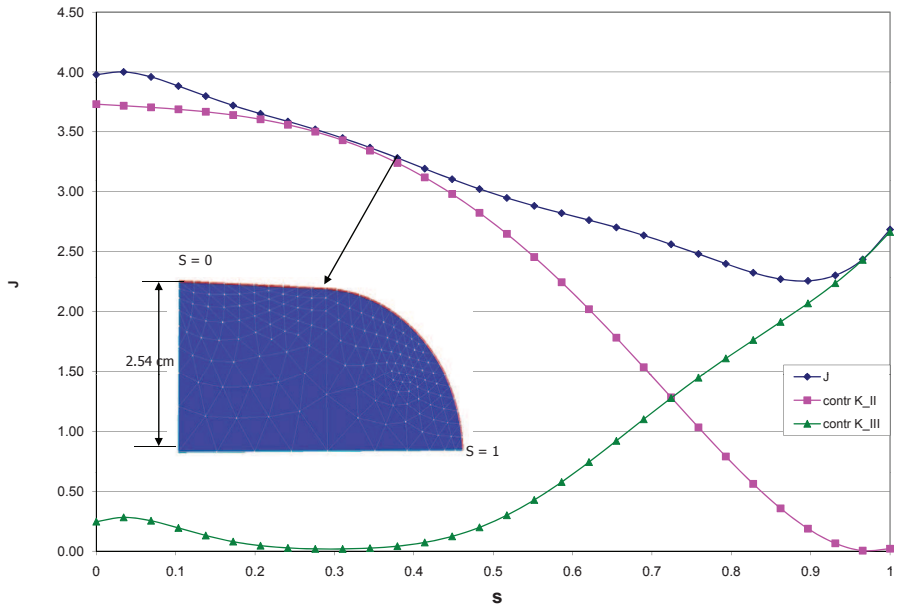

Figure 15. *Energy contributions from 3 Modes for load position B.*

6. Conclusions

From the analysis presented herein, it is clear that reflective cracks in airfield pavements are subjected to mixed mode behavior with all three modes present and thus, realistic simulations must be performed in three-dimensions. Such 3D analyzes can be used to determine if the crack will propagate towards the pavement surface or across the pavement, in a channeling orientation. This information may aid in the design of preventive measures against reflective crack growth and in the determination of critical parameters controlling their propagation. Three-dimensional simulations are also able to model the actual load distributions based on aircraft gear without the introduction of two-dimensional simplifications (calibration factors).

The mixed mode behavior demonstrated in this study will lead to non-planar crack growth which makes the simulation of this class of problems quite challenging for standard finite element methods. The generalized finite element removes some of the barriers faced by the FEM while retaining its attractive features. The simulation of three-dimensional crack growth in airfield pavements is currently the subject of our on-going research.

Acknowledgments/Disclaimer This paper was prepared from a study conducted in the Center of Excellence for Airport Technology. Funding for the Center of Excellence is provided in part by the Federal Aviation Administration under Research Grant Number 95-C-001. The Center of Excellence is maintained at the University of Illinois at Urbana-Champaign in the Department of Civil and Environmental Engineering who works in partnership with the Federal Aviation Administration. Ms. Patricia Watts is the FAA Program Manager for Air Transportation Centers of Excellence and Dr. Satish Agrawal is the Manager of the FAA Airport Technology R&D Branch. The contents of this paper reflect the views of the authors who are responsible for the facts and accuracy of the data presented within. The contents do not necessarily reflect the official views and policies of the Federal Aviation Administration. This paper does not constitute a standard, specification, or regulation.

7. Bibliographie

[AAS09a] « AASHTO M 320-09, "Performance-Graded Asphalt Binder", Standard Specifications for Transportation Materials and Methods of Sampling and Testing », 2009, 29th Edition.

[AAS09b] « AASHTO T322-07, "Standard Test Method for Determining the Creep Compliance and Strength of Hot Mix Asphalt (HMA) Using the Indirect Tensile Test Device", Standard Specifications for Transportation Materials and Methods of Sampling and Testing », 2009, 29th Edition.

[ADM 95] ADMINISTRATION(FAA) F. A., « Advisory circular : Airport pavement design for Boeing 777 airplane », rapport n° AC No. 150/5320-16, 1995, Department of Transportation, Washington, DC.

[BAB 94] BABUŠKA I., CALOZ G., OSBORN J., « Special Finite Element Methods for a Class of Second Order Elliptic Problems with Rough Coefficients », *SIAM Journal on Numerical Analysis*, vol. 31, n° 4, 1994, p. 945–981.

[BAB 97] BABUŠKA I., MELENK J., « The partition of unity finite element method », *International Journal for Numerical Methods in Engineering*, vol. 40, 1997, p. 727–758.

[BAE 08] BAEK J., AL-QADI I., XIE W., BUTTLAR W., « In-Situ Assessment of Interlayer Systems to Abate Reflective Cracking in Hot-Mix Asphalt Overlays », *Journal of the Transportation Research Board, National Research Council, Washington, D.C.*, , n° 2084, 2008, p. 104-113.

[BOZ 02] BOZKURT D., BUTTLAR W., « Three-Dimensional Finite Element Modeling to Evaluate Benefits of Interlayer Stress Absorbing Composite for Reflective Crack Mitigation », *Airport Technology Transfer Conference, Federal Aviation Administration*, , 2002.

[DAV 07] DAVE E., SONG S. H., PAULINO G. H., BUTTLAR W., « Integrated Testing and Modeling Approach for the Study of Reflective Cracking », *Proceedings of the Conference on Advanced Characterization of Pavement and Soil Engineering Materials*, Athens, Greece, 2007, p. 1241-1252.

[DAV 10] DAVE E., BUTTLAR W. G., « Thermal Reflective Cracking of Asphalt Concrete Overlays », *International Journal of Pavement Engineering*, , 2010, In press.

[DUA 95] DUARTE C., ODEN J., « Hp Clouds–A Meshless Method to Solve Boundary-Value Problems », rapport n° 95-05, May 1995, TICAM, The University of Texas at Austin.

[DUA 96a] DUARTE C., « *The hp Cloud Method* », PhD dissertation, The University of Texas at Austin, December 1996, Austin, TX, USA.

[DUA 96b] DUARTE C., ODEN J., « An *hp* Adaptive Method Using Clouds », *Computer Methods in Applied Mechanics and Engineering*, vol. 139, 1996, p. 237–262.

[DUA 96c] DUARTE C., ODEN J., « *Hp* Clouds – An *hp* Meshless Method », *Numerical Methods for Partial Differential Equations*, vol. 12, 1996, p. 673–705.

[DUA 00] DUARTE C., BABUŠKA I., ODEN J., « Generalized Finite Element Methods for Three Dimensional Structural Mechanics Problems », *Computers and Structures*, vol. 77, 2000, p. 215–232.

[DUA 01] DUARTE C., HAMZEH O., LISZKA T., TWORZYDLO W., « A Generalized Finite Element Method for the Simulation of Three-Dimensional Dynamic Crack Propagation », *Computer Methods in Applied Mechanics and Engineering*, vol. 190, n° 15-17, 2001, p. 2227–2262, http ://dx.doi.org/10.1016/S0045-7825(00)00233-4.

[KIM 02] KIM J., BUTTLAR W., « Analysis of Reflective Crack Control System Involving Reinforcing Grid over Base-Isolating Interlayer Mixture », *ASCE Journal of Transportation Engineering*, vol. 28, n° 4, 2002, p. 375-384.

[MEL 96] MELENK J., BABUŠKA I., « The partition of unity finite element method : Basic theory and applications », *Computer Methods in Applied Mechanics and Engineering*, vol. 139, 1996, p. 289–314.

[MOÕ9] MOËS N., DOLBOW J., BELYTSCHKO T., « A Finite Element Method for Crack Growth without Remeshing », *International Journal for Numerical Methods in Engineering*, vol. 46, 1999, p. 131-150.

[MOÕ2] MOËS N., GRAVOUIL A., BELYTSCHKO T., « Non-planar 3D crack growth by the extended finite element and level sets – Part I : Mechanical model », *International Journal for Numerical Methods in Engineering*, vol. 53, n° 11, 2002, p. 2549–2568.

[ODE 98] ODEN J., DUARTE C., ZIENKIEWICZ O., « A New Cloud-Based *hp* Finite Element Method », *Computer Methods in Applied Mechanics and Engineering*, vol. 153, 1998, p. 117–126.

[PAT] PATRAN, MSC Software, http ://www.mscsoftware.com/products/patran.cfm.

[PER 05] PEREIRA J., DUARTE C., « Extraction of Stress Intensity Factors from Generalized Finite Element Solutions », *Engineering Analysis with Boundary Elements*, vol. 29, 2005, p. 397–413.

[PER 09a] PEREIRA J., DUARTE C., GUOY D., JIAO X., « *Hp*-Generalized FEM and crack surface representation for non-planar 3-D cracks », *International Journal for Numerical Methods in Engineering*, vol. 77, n° 5, 2009, p. 601–633, http ://dx.doi.org/10.1002/nme.2419.

[PER 09b] PEREIRA J., DUARTE C., JIAO X., GUOY D., « Generalized finite element method enrichment functions for curved singularities in 3D fracture mechanics problems », *Computational Mechanics*, vol. 44, n° 1, 2009, p. 73-92, http ://dx.doi.org/10.1007/s00466-008-0356-1.

[STR 01] STROUBOULIS T., COPPS K., BABUŠKA I., « The Generalized Finite Element Method », *Computer Methods in Applied Mechanics and Engineering*, vol. 190, 2001, p. 4081–4193.

[SUK 00] SUKUMAR N., MOËS N., MORAN B., BELYTSCHKO T., « Extended Finite Element Method for Three-Dimensional Crack Modelling », *International Journal for Numerical Methods in Engineering*, vol. 48, n° 11, 2000, p. 1549–1570.

[SZA 88] SZABO B. A., BABUŠKA I., « Computation of the Amplitude of Stress Singular Terms for Cracks and Reentrant Corners », CRUSE T., Ed., *Fracture Mechanics : Nineteenth Symposium, ASTM STP 969*, Southwest Research Institute, San Antonio, TX, 1988, p. 101–124.

[TAD 00] TADA H., PARIS P., IRWIN G., *The Stress Analysis of Cracks Handbook*, ASME Press, New York, 3rd édition, 2000.